ELSEVIER

Earth and Planetary Science Letters 193 (2001) 115–127

EPSL

www.elsevier.com/locate/epsl

Evidence of hydration of the mantle wedge and its role in the exhumation of eclogites

Stéphane Guillot [a,*], Kéiko H. Hattori [b], Julia de Sigoyer [c], Thomas Nägler [d], Anne-Line Auzende [e]

[a] *Laboratoire de Dynamique de la Lithosphère, CNRS, UCB-Lyon et ENS-Lyon, 27 bd du 11 Novembre, 69622 Villeurbanne, France*
[b] *Department of Earth Sciences, University of Ottawa, Ottawa, ON, Canada K1N 6N5*
[c] *Laboratoire de Géologie, CNRS, ENS-Paris, 24 rue Lhomond, 75231 Paris Cedex 05, France*
[d] *Isotopengeologie, Erlachstrasse 9a, 3012 Bern, Switzerland*
[e] *Laboratoire 'Magmas et Volcans', CNRS, UBP-Clermont-Ferrand, 5 rue Kessler, 63038 Clermont-Ferrand, France*

Received 7 May 2001; received in revised form 27 August 2001; accepted 31 August 2001

Abstract

Serpentinite samples from the Indus suture zone, representing a shallower part of a paleo-subduction zone, show low-grade metamorphic recrystallization (chrysotile+magnetite ± magnesite ± talc). They are cumulates of melts formed in the uppermost mantle or the base of the Nidar intra-oceanic arc. Serpentinite samples associated with the Tso Morari eclogitic unit, representing the more deeply subducted portion of a paleo-subduction zone, exhibit high-grade metamorphic recrystallization (antigorite+magnetite ± forsterite ± talc) and the trace element chemistry of these samples suggests a strongly depleted mantle wedge origin. Nd concentrations and εNd values show that fluids responsible for hydration of the mantle wedge were derived from subducting clastic sediments overlying Tethyan oceanic crust. The exhumation of eclogites requires a mechanically weak zone at the interface between the subducting plate and the mantle wedge. We suggest that serpentinites associated with the Tso Morari eclogites acted as a lubricant for the exhumation of the eclogitic unit. Geophysical data suggest common occurrences of hydrated ultramafic rocks about 10 km thick along the interface between the mantle wedge and the subducting plate. We propose that such a low-viscosity zone played an important role for the exhumation of eclogitic rocks.

Keywords: serpentinite; eclogites; exhumation; mantle; Himalayas

1. Introduction

Mountain belts worldwide commonly contain eclogitic unit. *P–T–t* studies of such metamorphic rocks suggest that they were metamorphosed at depths of 50–150 km in subduction zones and exhumed to the surface at rapid rates of ∼1 cm/yr [1,2]. Various models have been proposed to explain the exhumation, but none of them satisfactorily explains all the geological and geophysical constraints (e.g. [1] for a review). Hydrated sediments may facilitate the exhumation of blueschists and low-pressure eclogites in the accretion-

* Corresponding author. Tel.: +33-72-44 62 41; Fax: +33-472-44 85 93.
E-mail address: sguillot@univ-lyon1.fr (S. Guillot).

0012-821X/01/$ – see front matter
PII: S0012-821X(01)00490-3

ary wedge (< 20 kbar), as large quantities of metasedimentary rocks commonly are intercalated with such high-pressure rocks. This was first proposed by Cloos [3] for rocks in the Franciscan Complex, California and supported by the evidence from many other places [4]. At greater depths, sediments are less abundant, and would not play a significant role for the exhumation of high-pressure to ultrahigh-pressure eclogitic rocks (> 20–25 kbar).

Subducting sediments and altered oceanic crust progressively release water, first during the porosity collapse at shallow depths and later due to dehydration reactions. Such fluids may hydrate the overlying mantle wedge [5]. Furthermore, serpentinite diapirs in the Mariana and Izu–Bonin forearcs [6] provide evidence of mantle wedge hydration. Hydration can profoundly alter the rheology of mantle rocks, and serpentinites formed in the mantle wedge may act as a lubricant for the exhumation of eclogites [7,8]. This paper presents the composition and mineral chemistry of serpentinites associated with the Tso Morari eclogitic unit in eastern Ladakh, NW Himalaya, and compares the results with those of serpentinites from the Indus suture zone representing two different levels of a paleo-subduction zone. Then we evaluate the origins of serpentinites and discuss the role of serpentinites in the exhumation of eclogitic unit.

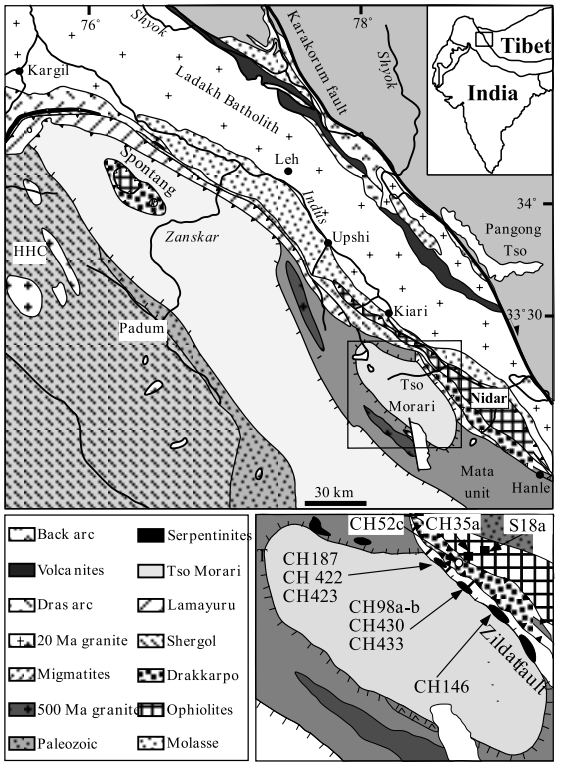

Fig. 1. Geological map of Ladakh–Zanskar (NW India), based on field work and satellite image analysis, showing the location of the Tso Morari eclogitic unit and its relationship with the Indus suture zone. Inset keys correspond to Himalaya–Karakorum belt and detailed geological map of the eastern Ladakh showing Tso Morari eclogitic unit and serpentinites. Sample locations are shown with arrows.

2. Regional geology

The eastern part of Ladakh (NW Himalaya, India) exposes from north to south the Ladakh calc-alkaline batholith, the Indus suture zone, and the Tso Morari unit (Fig. 1). The suture zone consists of Tertiary clastic sedimentary rocks, the Nidar arc complex, and the Drakkarpo tectonic melange. The suture zone is separated from the Tso Morari unit by the Zildat normal fault (Fig. 1). The Tso Morari 100×50 km eclogitic unit formed from the subducted Indian continental margin in late Paleocene time [9]. The Ladakh area is considered to be a subduction complex related to the closure of Neo-Tethys and the subduction of the Indian continental margin. Two north-dipping subduction zones were active simultaneously. The northern one corresponds to the subduction of Neo-Tethys, which resulted in the development of the Dras arc and the related Ladakh batholith. The southern subduction produced an oceanic arc (Nidar and Spontang ophiolites) that was later obducted over the Indian margin during early Paleocene time [10]. At the Paleocene–Eocene boundary, the Indian margin was subducted to depths greater than 70 km along the southern subduction zone, and was partly exhumed to form the Tso Morari unit [8,11].

In the Indus suture zone, serpentinites crop out at the base of the Nidar ophiolitic complex and in the Drakkarpo unit. These units and the serpen-

tinites record only greenschist-facies metamorphic conditions. Serpentinites also occur as intensely deformed, discontinuous lenses of $\sim 100 \times 1000$ m within the Zildat normal fault. They are intercalated with retrograded eclogitic lenses [7] and the style of deformation, including the top-to-the-northeast normal shearing, is very similar to that in the Tso Morari unit under amphibolitic- and greenschist-facies conditions. Field evidence suggests that eclogite as a large tectonic block formed earlier at great depth and was transported by serpentinite into the shallow crust [7], as observed in Catalina Island, California [4].

3. Sampling and analytical methods

Samples TS18c and CH35a were collected from the lower part of the Nidar arc (Fig. 1). Sample CH52c is from the Drakkarpo unit. Eight samples were collected from the Zildat normal fault in contact with the Tso Morari eclogites. Three samples (CH187, CH422, CH423) were obtained from the Ribil Valley, four samples (CH98a, CH98b, CH430, CH433) from the upper Sumdo Valley and sample CH146 from the Challung crest (Fig. 1). Major and minor element concentrations were determined using a Philips PW 2400 X-ray fluorescent spectrometer. Rhenium and platinum group elements (PGEs) were determined by isotopic dilution technique with a spike of ^{185}Re, and a mixed spike of ^{105}Pd, ^{190}Os, ^{191}Ir, and ^{194}Pt. Rhenium was separated using anion resin after digestion of samples. PGEs pre-concentrated into a Ni bead were dissolved in HNO_3. Mass ratios were determined using a HP4500 inductively coupled plasma mass spectrometer. Blanks were 0.04–0.1 ng Re, 0.002–0.007 ng Ir/g flux, 0.002–0.006 ng Os/g flux, 0.07–16 ng Pt/g flux and 0.03–0.9 ng Pd/g flux, negligible compared to the sample amounts; thus blank corrections were not applied to the results. For Nd isotope analysis, $\sim$100 mg of sample was digested after adding a mixed ^{150}Nd–^{149}Sm spike. Neodymium and Sm were separated using alkali resin followed by Teflon resin coated with HDEPH. Nd isotope compositions were determined using a single Re filament (NdO^+ emission) in a modified AVCO mass spectrometer. The oxygen isotope corrections were obtained by analyzing a ^{150}Nd spike as described in [12]. ^{143}Nd/^{144}Nd ratios were normalized against ^{146}Nd/^{144}Nd = 0.7219. During data acquisition, the La Jolla standard yielded ^{143}Nd/^{144}Nd = 0.511860 ± 0.000034. The concentration of Sm was determined using a triple Ta–Re–Ta filament. The blanks are 10 pg for Sm and 50 pg for Nd, negligible compared to sample sizes. Mineral compositions were determined using a Cameca CAMEBAX SX100 microprobe with a counting time of 10 s/element, 20 kV accelerating potential, and 20 nA sample current. Standards used were albite (Si), MgO (Mg), Al_2O_3 (Al), Cr_2O_3 (Cr), Fe_2O_3 (Fe), $TiMnO_3$ (Ti, Mn), vanadinite (V), NiO (Ni) and Co metal (Co).

4. Petrology of serpentinites

All samples are moderately to intensely sheared and consist predominantly of serpentines and magnetite, with a few relict textures of olivine and pyroxene. Unpublished X-ray diffractometer patterns and Raman spectroscopy suggest that the serpentines are predominantly antigorite with minor chrysotile and chlorite. Sample CH52c contains significant carbonates+chlorite and samples CH35a and TS18c consist predominantly of antigorite+chrysotile+magnetite in the matrix and millimeter-scale veinlets of magnetite ± talc. At least two stages of serpentinization are recognized in the Zildat serpentinites; the earlier one is characterized by the crystallization of blade-shaped antigorite and magnetite rimming Cr-spinel. Later serpentinites are undulating sheets of antigorite and/or chrysotile replacing pyroxene or form millimeter-scale veinlets together with magnesite+talc+magnetite. The earlier blades of antigorite are locally surrounded by tabular olivine (several mm in length), which constitutes 5–20 vol% of the thin sections. Minor amounts of talc occur as minute acicular crystals with olivine. Several olivine crystals in sample CH433 are surrounded by late serpentine+magnesite. Chromite in the Nidar and Zildat samples has relatively high Cr_2O_3 (48–58 wt%), with variable X_{Cr} (atomic ratio of Cr/[Cr+Al]) ranging from 0.55 to 0.84 (Table 1) and

Table 1
Representative microprobe analyses of olivine and Cr-spinel

Mineral sample	Olivine CH98b	Olivine CH98a	Olivine CH430	Olivine CH423		Spinel CH35a	Spinel CH98a	Spinel CH98b	Spinel CH146	Spinel CH423	Spinel CH422	Spinel CH430	Spinel CH433
SiO_2	42.73	43.61	43.45	42.56	SiO_2	0.03	0.02	0.00	0.00	0.05	0.06	0.00	0.05
TiO_2	0.04	0.03	0.00	0.04	TiO_2	0.10	0.04	0.04	0.19	0.15	0.11	0.58	0.12
FeO	3.81	1.32	2.05	2.12	Al_2O_3	18.80	8.82	9.29	6.66	7.45	11.31	9.26	18.10
Cr_2O_3	0.00	0.00	0.00	0.00	Cr_2O_3	42.67	57.07	58.74	53.49	54.84	53.08	50.21	47.51
MgO	54.78	54.33	54.12	54.99	Fe_2O_3	7.33	3.82	2.92	9.94	7.71	5.79	10.49	4.09
MnO	0.16	0.22	0.16	0.14	FeO	27.45	22.90	21.70	23.00	22.77	22.59	16.58	20.90
NiO	0.00	0.00	0.00	0.00	MgO	7.88	6.74	7.72	6.30	6.05	6.86	7.08	8.77
CaO	0.02	0.03	0.01	0.01	MnO	0.68	0.00	0.00	0.00	0.81	0.49	4.17	0.40
NiO	0.00	0.00	0.00	0.00	NiO	0.09	0.03	0.05	0.05	0.04	0.05	0.08	0.06
					ZnO	0.02	0.00	0.16	0.29	0.34	0.41	1.98	0.13
Total	101.48	99.54	99.79	99.87	total	100.25	99.64	100.84	100.13	100.73	100.76	100.42	100.17
Calc. based on 4 O					Calc. based on 32 O								
Si	1.00	1.03	1.02	1.00	Si	0.00	0.00	0.00	0.00	0.00	0.00	0.00	0.00
Ti	0.00	0.00	0.00	0.00	Ti	0.00	0.01	0.01	0.04	0.03	0.02	0.12	0.02
Fe	0.08	0.03	0.05	0.04	Al	5.77	2.85	2.94	2.17	2.42	3.57	2.96	5.50
Mg	1.91	1.92	1.91	1.94	Cr	8.78	12.36	12.46	11.71	11.95	11.24	10.78	9.68
Mn	0.00	0.00	0.00	0.00	Fe^{3+}	1.44	0.79	0.59	2.07	1.60	1.17	2.14	0.79
Ni	0.00	0.00	0.00	0.00	Fe^{2+}	4.77	5.24	4.87	5.33	5.25	5.06	3.76	4.51
Al	0.00	0.00	0.00	0.00	Mg^{2+}	3.06	2.75	3.09	2.60	2.48	2.74	2.87	3.37
Ca	0.00	0.00	0.00	0.00	Mn^{2+}	0.15	0.00	0.00	0.00	0.19	0.11	0.96	0.09
Total	3.00	2.98	2.98	2.99	Ni^{2+}	0.02	0.01	0.01	0.01	0.01	0.01	0.02	0.01
					Zn^{2+}	0.00	0.00	0.03	0.06	0.07	0.08	0.40	0.03
% Fo	96.2	98.7	97.9	97.9									
					Cr#	0.60	0.81	0.81	0.84	0.83	0.76	0.78	0.64
					Mg#	0.39	0.34	0.39	0.33	0.32	0.35	0.43	0.43

low and Fe_2O_3 (3–10 wt%). The Cr-spinels from the Nidar ophiolite have the lowest X_{Cr}, $\sim$0.6, whereas those from the Zildat samples have higher X_{Cr} of $\sim$0.8 due to lower Al_2O_3, $<$19.2 wt% (Table 1). The X_{Mg} values (atomic ratios of Mg/[Mg+Fe^{2+}]) are similar (0.33–0.41) in all samples. A plot of X_{Cr} vs. X_{Mg} shows that the samples are similar to those of arc settings, including those from the southeast Alaskan complex [13] and the Jijal complex in Pakistan [14] (Fig. 2). Our chromites are distinctly different from those in abyssal peridotites [15]. Olivine contains high MgO (Fo_{96-98}) (Table 1), much greater than olivine in the mantle ($<Fo_{95}$) [16]. The MgO contents are much higher than those expected from the olivine–chromite mantle array [16], suggesting that the olivine is not in equilibrium with the associated chromite and is of metamorphic origin. The assemblage of talc+olivine at the expense of antigorite may develop under two different conditions [17] (Fig. 3):

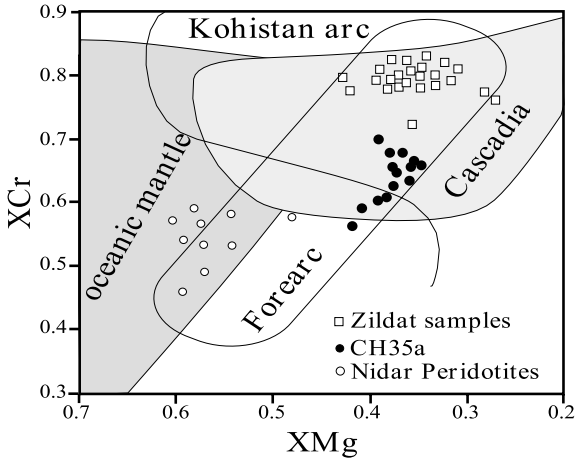

Fig. 2. Composition of cores of chromian spinels. X_{Cr} = atomic ratios of Cr/(Cr+Al), X_{Mg} = atomic ratios of Mg/(Mg+Fe^{2+}). The spinel compositions from the Zildat samples fall in the supra-subduction zone field, suggesting a depleted mantle source, whereas the spinel compositions from the Nidar sample CH35a fall in the fields of both supra-subduction zones and of oceanic abyssal peridotites, suggesting a less depleted mantle source.

31 antigorite + 33 enstatite = 2 forsterite + 31 talc (1)

14 antigorite = 18 forsterite + 4 talc + 20 H_2O (2)

As the Tso Morari eclogites record peak metamorphic conditions of 21–24 kbar and 550–600°C [11], the forsterite+talc assemblage could have first developed in the Zildat serpentines during decompression (Eq. 1). The assemblage could also have developed later by temperature increase at depths of about 30–35 km during the exhumation (Eq. 2, Fig. 3). Talc is not abundant in the samples and forsterite forms around antigorite, suggesting that development of the forsterite+talc assemblage occurred through Eq. 2. A late hydration produced further serpentinization. The late magnesite+talc veinlets developed in both the Zildat and the Indus suture zone samples are commonly developed during low-temperature carbonatization [17] (Fig. 3);

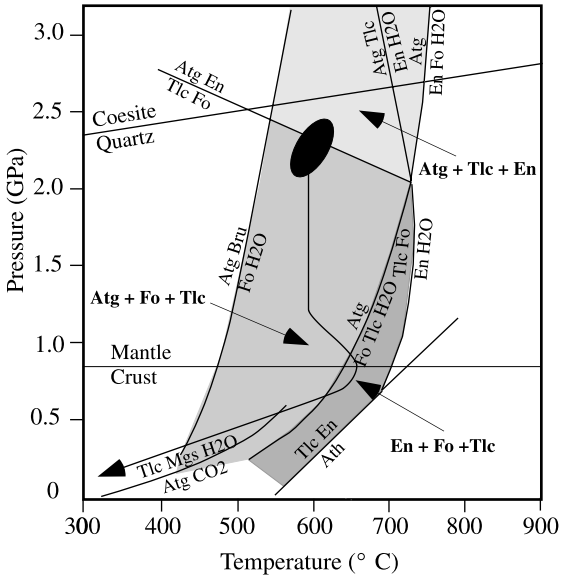

Fig. 3. Phase relationships in the MgO–SiO_2–H_2O–CO_2 system, modified after [17,36]. Atg = antigorite, Ath = anthophyllite, Bru = brucite, En = enstatite, Fo = forsterite, Mgs = magnesite, Tlc = talc. The shaded areas corresponds to the different serpentinite mineral associations (Tlc ± Atg ± Fo ± En) crossed by the Tso Morari *P–T* path [11].

24 forsterite + 31 H_2O + 20 CO_2 =

antigorite + 20 magnesite (3)

2 antigorite + 45 CO_2 =

17 talc + 45 magnesite + 45 H_2O (4)

5. Bulk chemical composition of serpentinites

Serpentinites contain low concentrations of incompatible elements, which are useful in evaluating the origin of igneous rocks. In addition, many incompatible elements are mobile during serpentinization, which makes it difficult to identify their protoliths [18]. Fortunately, serpentinites contain significant contents of transition elements, which are generally immobile during metasomatism [19]. In addition, they contain high concentrations of PGEs which may be used to discriminate the origins of serpentinites. Most of our samples (Zildat samples and CH35a) contain high Cr (>2000 ppm), Ni (>2000 ppm), and MgO (>41 wt%), and low Al_2O_3 (<1.0 wt%) and CaO (<1.0 wt%) (Table 2). Low contents of CaO may be attributed to the dissolution of clinopyroxene during serpentinization, but very low contents of Al_2O_3 together with high Cr suggest that the original rocks were dunite or harzburgite. Furthermore, these rocks contain low concentrations of mildly incompatible elements, such as Ti and V (Fig. 4), suggesting that they were derived from mantle residues. The residual mantle origin of the Zildat serpentinites and TS18c is also confirmed by the ratios Ti/Cr vs. V/Cr and Ti/Cr vs. Al/Cr (Fig. 5). In contrast, samples CH52c and TS18c contain low Ni and MgO, and high Al_2O_3 (9.4–19 wt%) and CaO (3.6–5.1 wt%), consistent with the occurrence of chlorite and relict plagioclase. The compositions suggest that they are solidified melt in the uppermost mantle or lower crust. This is further supported by high concentrations of moderately incompatible Ti and V relative to primitive mantle values (Fig. 4). Sample CH52c contains high concentration of Y (34 ppm) and Zr (81 ppm). Sample CH52c was collected at the base of Drakkarpo unit, which is interpreted to be an

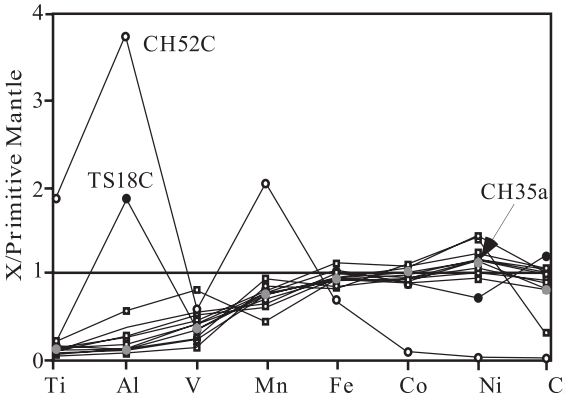

Fig. 4. Primitive mantle-normalized immobile elements. Samples CH52c and TS18c are enriched in relatively incompatible elements and depleted in compatible elements, whereas the Zildat samples and CH35a are depleted in incompatible elements and slightly enriched in compatible elements, typical of a depleted mantle. Primitive mantle values are from [47].

oceanic island [7]. It likely represents a cumulate of oceanic basalts, which are enriched in Y and Zr (Table 2).

6. Rhenium and PGEs

PGEs are divided into two groups: Pt-type (Pt, Pd, Rh) and Ir-type (Ir, Os, Ru). The latter elements are compatible during partial melting and are retained in the mantle, whereas the former elements may be enriched in melts. The contents of PGEs and Re in the serpentine samples show two patterns. Samples CH52c and TS18c show low concentrations of Os and Ir and high ratios of Pt-type/Ir-type PGEs. The rest of the samples show high concentrations of Os and Ir and low ratios of Pt-type/Ir-type, displaying a flat, primitive mantle-normalized pattern (Fig. 6). Several

Table 2
Bulk chemical composition of serpentinite samples

Sample	CH35a	CH52c	CH98a	CH98b	CH146	CH187	TS18c	CH422	CH423	CH430	CH432	CH433
SiO_2 (wt%)	38.68	29.55	35.05	40.15	40.59	39.39	38.09	39.6	37.4	43.16	39.38	39.18
TiO_2	0.02	0.37	0.03	0.02	0.02	0.02	0.03	0.02	0.01	0.04	0.01	0.01
Al_2O_3	0.49	16.72	0.54	0.37	0.77	1.09	8.44	1.6	0.31	2.53	1.18	0.56
Fe_2O_3 (t)	7.58	5.55	6.83	7.54	7.59	8.99	8.19	7.993	6.604	7.289	7.58	7.388
MnO	10.00	28.00	13.00	10.00	0.09	0.11	0.11	0.09	0.12	0.06	0.08	0.10
MgO	38.56	29.65	39.97	41.82	36.65	38.00	30.59	37.00	41.86	34.28	37.83	37.49
CaO	0.65	4.41	0.64	0.29	1.05	0.33	3.22	0.48	0.2	0.45	0.64	1.4
Na_2O	<0.005	<0.005	<0.005	<0.005	<0.005	<0.005	0.16	<0.0	<0.0	<0.0	<0.0	<0.0
K_2O	<0.005	<0.005	<0.005	<0.005	<0.005	<0.005	0.01	<0.0	<0.0	<0.0	<0.0	<0.0
P_2O_5	0.00	0.08	0.01	0.01	0.00	<0.001	0.00	0.01	0.02	0.01	0.01	0.01
LOI	13.8	14.7	17.00	9.8	13.1	11.8	11.1	13.1	13.2	11.6	12.8	13.5
Cr (ppm)	2121	32	2718	2604	2581	2778	3159	2293	768	2640	2157	2373
V	28	48	19	18	34	37	27	45	11	66	42	34
Co	107	<10	97	110	93	113	94	100	114	101	92	97
Zn	49	21	51	54	30	32	45	34	27	32	24	44
Ni	2222	16	2255	2825	2260	2393	1387	2064	2762	2285	1852	1977
Ga	<10	13	<10	<10	<10	<10	<10	<1.0	<1.0	2.2	1.8	<0.0
Zr	<5	69	<5	<5	<5	<5	<5	2	<1	2	4	4
Y	<5	29	<5	<5	<5	<5	<5	<0.0	<0.0	<0.0	<0.0	<0.0
Sr	10	28	24	12	17	5	36	7	4	19	18	54
Pb	140	<10	450	111	<15	315	15	93	93	135	85	261
Th	<10	<10	14	<10	<10	11	<10	<0.0	<1.00	<0.0	2.35	<0.0
U	<10	<10	30	<10	<10	17	<10	<0.0	<0.0	2	11	6
Os (ppb)	2.2	0.08	3.77	1.4	3.00	1.6	0.27	3.17	5.24	3.19	3.45	3.24
Ir	2.25	0.041	1.53	2.95	1.39	2.83	0.19	2.41	4.29	3.07	2.72	4.32
Pt	2.1	1.2285	1.4635	6.8075	5.0735	5.467	2.03	10.51	2.63	5.48	34.82	1055
Pd	8.36	11.80	2.23	4.69	2.84	20.10	5.82	4.36	3.29	9.94	4.36	3.90
Re	0.01	0.01	0.01	0.02	0.03	0.20	0.08	0.04	0.01	0.04	0.08	0.04
Total (wt%)	100.33	101.32	100.70	100.65	100.36	100.26	100.40	100.13	100.03	99.70	99.74	99.93

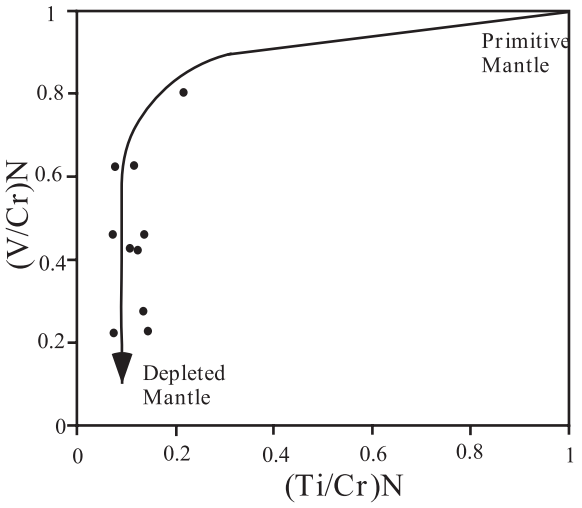

Fig. 5. Primitive mantle-normalized elemental ratios: (Ti/Cr)N vs. (Al/Cr)N and (Ti/Cr)N vs. (V/Cr)N. The Zildat serpentinites and CH35a show strong depletion of incompatible elements compared to primitive mantle, suggesting derivation from a depleted mantle source.

samples show a moderate enrichment of Pd, which may be attributed to serpentinization because Pd is relatively mobile in saline fluids [19]. The concentrations of PGEs and ratios of Pd/Ir and Pt/Ir for all the samples except CH52c and TS18c are all similar to those of mantle xenoliths [20] and ultramafic massifs, such as Ronda and Beni Bousera [21]. The PGE data, therefore, suggest a mantle origin for the samples. Rhenium is incompatible during partial melting [22]. Thus the

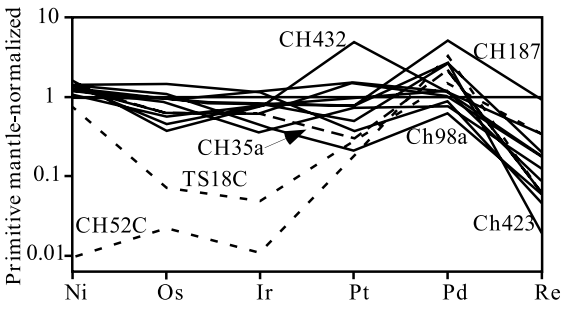

Fig. 6. Primitive mantle-normalized plot of Ni, PGE and Re contents in serpentinites. Primitive mantle values are 1960 ppm for Ni and 0.28 ppb for Re [47]. The values for PGE in primitive mantle are 0.00725 times those of CI chondrite values [47]: 3.55 ppb Os, 3.30 ppb Ir, 7.32 ppb Pt, and 3.99 ppb Pd.

Table 3
Nd isotopic compositions for selected Zildat serpentinites

Sample	Sm ppm	Nd ppm	$^{143}Nd/^{144}Nd$	εNd(0)
CH98a	0.0185	0.058	0.512507 ± 31	−2.6
CH98b	0.0213	0.0763	0.512263 ± 41	−7.3
CH146	0.0194	0.049	0.512753 ± 52	+2.2
CH187	0.0185	0.041	0.512439 ± 64	−3.9
CH422	0.04	0.1313	0.511898 ± 22	−14.4
CH433	0.0408	0.1516	0.511612 ± 23	−20.0

low Re suggests that the Zidalt samples and CH35a represent mantle residues. The samples contain high Os and Ir and low Al, and plot in the field of mantle residue (Fig. 7). In contrast, samples TS18c and CH52c contain low Os and Ir and high Pd and Pt (Table 2). Incompatible Re, Pt, and Pd may be enriched in magmas, whereas compatible Os and Ir remain in the mantle. Therefore, crustal rocks and even cumulates are generally low in Os and Ir. Examples include ultramafic cumulates of boninites at Heazelwoodite [23], dunite and wehrlite of the Talkeetna arc in Alaska [24], and the Kohistan arc in Pakistan

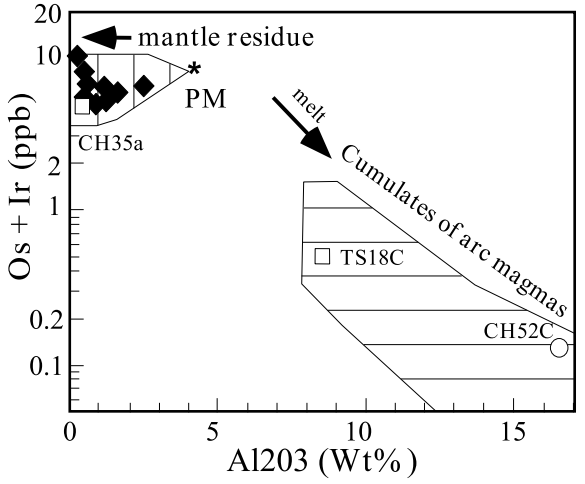

Fig. 7. (Ir+Os) vs. Al_2O_3 of serpentinites (solid diamonds) compared to ultramafic cumulates of the Jijal Complex, Pakistan, and the Talkeetna arc, Alaska (horizontally striped area) and rocks of abyssal peridotite, Ronda and Beni Bousera massifs (vertically striped area). Serpentinite samples plot in the field of refractory mantle residues, whereas the data from samples TS18c and CH52c are similar to those of crustal cumulates.

[25]. Highly fractionated PGEs patterns from TS18c and CH52c (Fig. 6) suggest their cumulate origin.

7. Neodymium isotope compositions of serpentinites

Neodymium isotopic compositions of Zildat serpentinites are determined to evaluate the source of fluids for serpentinization. The contents of Nd and Sm in the samples are low, less than 0.15 ppm (Table 3), but samples with higher Nd contents show lower εNd and high Nd/Sm ratios (Fig. 8). The linear array of 1/Nd and εNd suggests a mixing of two components. One end component with greater concentration of Nd has Nd/Sm ratios of ∼4 and an εNd value of ∼−25. The other component has a very low concentration of Nd, less than 0.04 ppm, low Nd/Sm ratios, and high εNd of ∼+10. The εNd values lower than −20 are indicative of Archean crustal metasediments, whereas high εNd values of ∼10 represent that of a depleted mantle [26]. Neodymium is incompatible during partial melting and preferentially enriched in the liquid. Therefore, low Nd concentrations, <0.04 ppm, are consistent with a depleted mantle source.

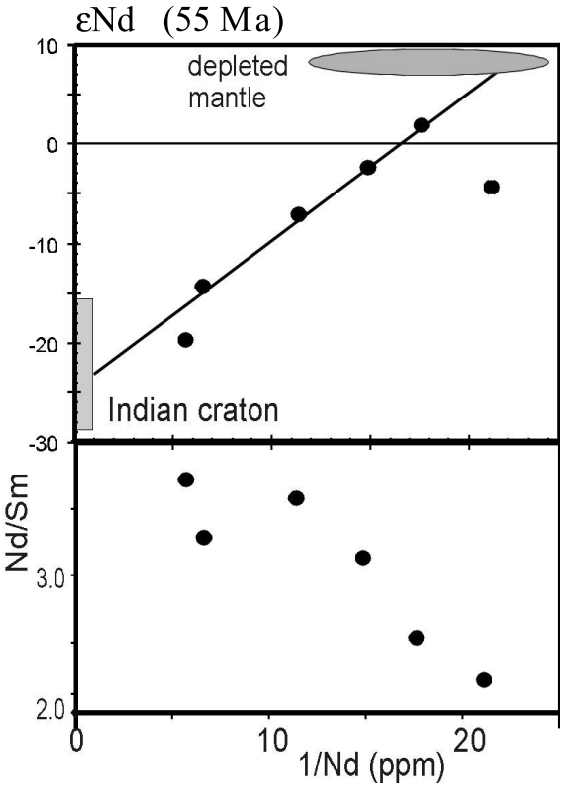

Fig. 8. εNd vs. 1/Nd diagram of six Zildat serpentinites. A linear correlation ($r=0.985$) for five out of six samples suggests a two-component mixing as the REE source. The end member with low concentration of Nd (<0.04 ppm) is superchondritic (positive εNd), in line with LREE-depleted mantle characteristics. The end member with high concentration shows Nd isotopic compositions typical for Precambrian continental crust (εNd < −19). This concentration (ca. 0.20 ppm Nd) is still very low compared to the concentration of Nd, 30–40 ppm, for continental crust. In addition, the bulk chemical compositions of the serpentinites do not allow a bulk addition of continental material. Instead, Nd in the samples was transported, resulting in the overprinting of the original mantle Nd isotope signature.

8. Discussion

8.1. Metamorphic conditions of Himalayan serpentinites

Serpentinite collected from the Indus suture zone displays evidence for only greenschist-facies metamorphic conditions. In contrast, Zildat serpentinites with metamorphic olivine+talc assemblage were metamorphosed at higher temperatures. The assemblage forsterite+talc+antigorite is stable under pressures ranging from 0.5 to 2.5 GPa at temperatures lower than 650°C, but it likely developed at a depth ranging between 35 and 70 km, considering the P–T path of the associated Tso Morari eclogites (Fig. 3). The occurrence of forsterite replacing antigorite suggests earlier serpentinization prior to the formation of metamorphic forsterite+talc in the mantle wedge.

8.2. Origin of the Himalayan serpentinites

The chromite chemistry, bulk chemical compositions, and concentration of PGEs suggest that samples CH52c and TS18c are cumulates from melts. In contrast, the other serpentinite samples show strongly refractory characters. Chromite of similar composition may occur in cumulates, but

the low Re and high Ir and Os contents rule out this possibility because ultramafic cumulates of arc magmas generally contain very little Os and Ir [24,25]. Except for CaO, concentration of major elements in the Zildat serpentinites are similar to harzburgites in the forearc of the Mariana Trough [27] and unaltered harzburgite [28]. Their low Al and Mn contents and high Co, Ni, and Cr contents also suggest harzburgitic origin. The high Cr# of the chromite from the Zildat serpentinites compared to the chromite from the Nidar–Spontang arc suggests that the protoliths of the Zildat serpentinites are more refractory than the latter, suggesting a mantle wedge origin.

8.3. Fluids responsible for hydration of Himalayan serpentinites

The mixing relationship between Nd concentration and εNd suggests two sources: a depleted mantle and Archean crust. The linear relationship between Nd concentration and Nd/Sm ratios suggests that the Nd with low εNd values (~ -25) had high Nd/Sm ratios. This is consistent with high Nd/Sm ratios of crustal rocks and the relatively soluble nature of Nd compared to Sm. Indeed, basement gneisses deriving from Archean sediments in the Himalaya have present-day εNd values ranging from -20 to -30 [29]. Fluids derived from subducting sediments overlying the Tethyan oceanic crust likely carried Nd with Archean crustal signatures.

8.4. Hydration of the mantle wedge and exhumation of eclogites

Serpentinites are commonly associated with eclogites in mountain belts such as the Alps [8,30,31]. This suggests a possible role of the serpentinites in the exhumation of eclogites. In the following sections, we discuss the evidence for hydration of the mantle wedge and a possible role for serpentinites in the exhumation of eclogites. The association of serpentinites and eclogites could occur in different tectonic settings. Serpentinites may be formed by hydration of a mantle diapir on the ocean floor during slow rifting of the oceanic crust [8]. Mafic igneous rocks formed in the mantle diapir would be subducted together with the surrounding serpentinized ultramafic rocks. Alternatively, the serpentinites may represent a portion of the mantle wedge that was tectonically juxtaposed against eclogitic rocks during exhumation. Thus, the origin of the ultramafic rocks (oceanic mantle diapir or mantle wedge), and the P–T conditions for serpentinization are crucial in evaluating the origin of the serpentinites.

In subduction zones, dewatering of sediments would hydrate mantle peridotites at depths greater than 10 km, and the water flux increases at the blueschist–eclogite transition, at $\sim$40 km depth [32]. There is abundant geological and geophysical evidence for the serpentinization of mantle wedges [33]. Examples include serpentinite diapirs in the Mariana forearc [6], and extensively serpentinized mantle rocks on Santa Catalina Island, California [4]. The occurrence of hydrated mantle is further supported by geophysical data from active subduction zones. First, a low-velocity layer 10 km thick with reduced frictional stress has been observed down to 70–100 km depth along the Japanese subduction zone [34], and P- and S-wave velocity models in central Japan suggest that Poisson's ratios greater than 0.3 at depths of 20–45 km are related to serpentinized peridotites [35]. Bailey and Holloway [36] suggested that a layer of partially hydrated peridotites would best explain the geophysical properties of the low-velocity layer. Second, high H_2O contents are suggested for high electric conductivities along the interface between the mantle wedge and the subducting slab [37]. Finally, the down-dip limit of the seismogenic zone may be explained by the deep occurrence of aseismic hydrous minerals such as antigorite or talc in the mantle wedge [33].

8.5. Physical characteristics of the hydrated mantle layer

We now describe the viscosity, density, and thickness of the hydrated mantle layer using numerical simulations and the exhumation rate of eclogites. Schwartz et al. [30] showed a return flow in a hydrated, soft layer with low density and viscosity, which would lead to an upward

viscous flow of rigid eclogitic blocks. Rocks with viscosity greater than $\sim 10^{20}$ Pas but less than $\sim 10^{23}$ Pas would allow the exhumation of an eclogitic block with a volume of ~ 50 km^3, whereas smaller eclogitic blocks could be exhumed at a lower viscosity, $< \sim 10^{20}$ Pas. Pure serpentinites have low viscosity, 10^{19} Pas [38]. Thus, the exhumation of a large eclogitic unit requires peridotite with 10–50% hydration, which has a density between 2800 and 3100 kg/m^3. Mass–balance calculation suggests the thickness of the partially hydrated layer as 10–20 km [30]. This is similar to the size of the low-velocity zone in active subduction zones [34,35].

The viscosity of the hydrated layer may also be constrained by comparing the relationship between exhumation rate, strain rate and convergent rate in different locations. In the Himalaya, during exhumation of the Tso Morari unit, the rate of convergence was between 18 and 10 cm/yr [39], whereas the exhumation rate of the Tso Morari eclogites within the mantle wedge was 0.5–1 cm/yr [9]. The exhumation rate in the Western Alps is higher (1.3 cm/yr) [40] than that in the Himalaya, although the convergent rate in the Alps, < 2 cm/yr [41], is much slower than that in the Himalaya. This suggests that the velocity of exhumation is independent of the velocity of the subducting plate, and more probably controlled by the strain rate of the exhumation zone:

$$V = \dot{\varepsilon}.Z/\sin\alpha$$

with V the velocity of exhumation, Z the height of the mantle wedge, α the dip of the subduction zone and ε the strain rate (Fig. 9). Considering that Z is equal to 35 km deduced from the minimum pressure recorded by the eclogites, V equal to 1 cm/yr in the Himalaya and the Alps and if α is fixed at 30°, a strain rate $\dot{\varepsilon}$ of 5×10^{-15} s^{-1} yields the observed exhumation velocity. As the strain rate is dependent on the Newtonian viscosity and the forces applied in the exhumation zone, we can estimate the Newtonian viscosity in the exhumation zone:

$$\mu = \sigma/\dot{\varepsilon}$$

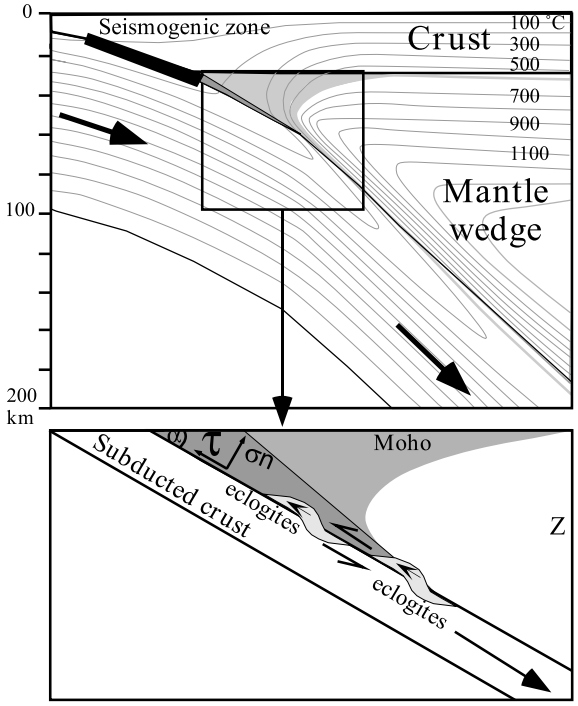

Fig. 9. Schematic cross-section of a subduction zone showing the potential area of forearc mantle serpentinization (gray area) at temperatures below 600°C, modified from [36]. The inset shows the region of forearc mantle serpentinization (light gray area) and the effective zone of 10-km-thick hydrated mantle that likely corresponds to the low-velocity zone. The eclogitization of the upper part of the subducting slab results in an increased rigidity of this zone and a downward shift of the main subducting shear plane to the boundary between the upper and lower crust of the subducting plate. The eclogitized block is then isolated and would be incorporated into the overlying serpentinites and would be entrained upward within the serpentinite channel.

where σ is the stress at the slab interface and $\dot{\varepsilon}$ the strain rate in the exhumation zone. For a stress equal to 20 ± 10 MPa at the interface between the mantle wedge and the subducting slab [42] and a strain rate equal to 5×10^{-15} s^{-1}, the Newtonian viscosity should range from 2 to 6×10^{21} Pas. This is two orders of magnitude lower than the viscosity of dry peridotite, but greater than that of a pure serpentinite, again suggesting partial hydration of the mantle wedge.

8.6. Role of serpentinites in the exhumation of eclogitic rocks

The exhumation of eclogitic unit requires an upward force greater than the downward force. The positive buoyancy developed by the density contrast between felsic eclogites (3100 kg/m^3) and dense surrounding mantle (3300 kg/m^3) is considered to be the primary cause of the exhumation [1]. In contrast, mafic eclogites are denser (3500 kg/m^3) than the peridotite in the deep mantle. Moreover, a dry mantle wedge is rigid with a high viscosity of about 10^{23} Pas [38], and a low strain rate, lower than 10^{-15} s^{-1} [43,44]. The resistance of the rigid mantle would be reduced by the existence of a mechanically weak zone along the subducting plate. Hydrated sediments have a viscosity $<10^{17}$ Pas [2] and can easily lubricate the interface between the two, to facilitate exhumation of high-pressure rocks greater than hundreds of meters in size, as documented in the Franciscan Complex [2]. At greater depths, >50 km, sedimentary accretionary wedges pinch out, and the abundance of sediments decreases significantly. A partially hydrated peridotitic layer containing antigorite+talc does contribute to the exhumation of eclogitic units such as the Tso Morari unit.

Experiments show that the strength of serpentinites decreases at temperatures between 400 and 600°C at various pressures, and that the ductility increases as pressure increases above 400 MPa at room temperatures [45]. Hydration of peridotites reduces the shear stress at high pressures (>40 km depth) due to decreased viscosity, from 10^{23} Pas to 10^{19} Pas at 550°C [43,44] and a high Poisson's ratio of about 0.34 [45]. The low density ($\sim$2600 kg/m^3) of serpentinites makes the entire unit containing mafic eclogites in a serpentinite matrix buoyant. Therefore, for these physical reasons, soft serpentinites between the subducting plate and the rigid mantle wedge at depths >40 km may facilitate the exhumation of eclogites.

The exhumation of eclogitic units requires the physical separation of the block from the subducting plate. The upper portion of the subducting plate is hotter than the lower portion. Thus, the eclogitization occurs first in the upper portion of subducting plates, which produces the disparity of strength in subducting plates [46] and a shear zone between the shallower and deeper portions of the subducting plates, which likely results in a downward shift of the main subducting shear plane to the boundary between the upper and lower crust of the subducting plates [46]. The eclogitized upper crustal block is then sandwiched between two shear zones and would be easily dislodged from the remaining subducting plate into the overlying serpentinites (Fig. 9). This allows an upward movement of the rigid eclogitic block in the ascending serpentinite layer.

9. Conclusions

Serpentinites from eastern Ladakh (India, NW Himalaya), a Tethyan paleo-subduction zone, originated from two different sources. Serpentinites from the Indus suture zone represent cumulates of melt and harzburgite, either at the base of Nidar arc or in the uppermost mantle. In contrast, serpentinites in close spatial association with the Tso Morari eclogitic unit were derived from a highly refractory mantle wedge. They were hydrated at depth by fluids released from subducting sediments on the Tethyan oceanic crust or subducting Indian continent. Considering the low viscosity, high Poisson's ratio and low density of serpentinites, it is likely that the serpentinites facilitated the exhumation of the Tso Morari eclogitic unit. Serpentinites occur together with many eclogitic rocks in active and past subduction zones worldwide, suggesting that serpentinites may have assisted the exhumation of eclogites elsewhere. The occurrence of hydrated mantle along subduction zones has been suggested from low seismic velocities, reduced frictional stress, and high electrical conductivity. We propose that a layer of antigorite+talc+forsterite, about 10 km thick, at the interface between the mantle wedge and subducting plate, could partly explain both the geophysical data and the exhumation of eclogites.

Acknowledgements

This study was supported by CNRS-France and NSERC-Canada. We thank Pascal Allemand for discussions and suggestions. Nicole Veschambre, Ron Hartree, and Monika Wilk-Alemany are thanked for their analytical assistance. We also thanks J.G. Liou, W.G. Ernst, S. King and an anonymous reviewer for constructive reviews. *[SK]*

References

[1] W.G. Ernst, J.G. Liou, Overview of UHP metamorphism and tectonics in well-studied collisional orogens, Int. Geol. Rev. 41 (1999) 477–493.
[2] J.G. Liou, D.A. Carswell, Garnet peridotites and ultrahigh-pressure minerals, J. Metamorph. Geol. 18 (2000) 181–192.
[3] M. Cloos, Flow melanges: numerical modelling and geological constraints on their origin in the Franciscan subduction complex, Geol. Soc. Am. Bull. 93 (1982) 330–345.
[4] P. Allemand, J.M. Lardeaux, Strain partioning and metamorphism in a deformable orogenic wedge application to the Alpine belt, Tectonophysics 280 (1997) 157–169.
[5] G.E. Bebout, M.D. Barton, Fluid flow and metasomatism in a subduction zone hydrothermal system: Catalina Schist terrane, California, Geology 17 (1989) 976–980.
[6] P. Fryer, C.G. Wheat, M.j. Mottl, Mariana blueschist mud volcanism implications for conditions within the subduction zone, Geology 13 (1999) 103–106.
[7] S. Guillot, K. Hattori, J. de Sigoyer, Mantle wedge serpentinization and exhumation of eclogites insights from eastern Ladakh, northwest Himalaya, Geology 28 (2000) 199–202.
[8] J. Hermann, O. Müntener, M. Scambelluri, The importance of serpentinite mylonites for subduction and exhumation of oceanic crust, Tectonophysics 327 (2000) 225–238.
[9] J. de Sigoyer, V. Chavagnac, J. Blichert-Toft, I.M. Villa, B. Luais, S. Guillot, M. Cosca, G. Mascle, Dating the Indian continental subduction and collisional thickening in the northwest Himalaya: multichronology of the Tso Morari eclogites, Geology 28 (2000) 487–490.
[10] G. Mahéo, H. Bertrand, S. Guillot, G. Mascle, A. Pêcher, C. Picard, J. de Sigoyer, Témoins d'un arc immature téthysien dans les ophiolites du Sud Ladakh (NW Himalaya, Inde), CR Acad. Sci. Paris 330 (2000) 289–295.
[11] S. Guillot, J. de Sigoyer, J.M. Lardeaux, G. Mascle, Eclogitic metasediments from the Tso Morari area (Ladakh, Himalaya): evidence for continental subduction during India-Asia convergence, Contrib. Mineral. Petrol. 128 (1997) 197–212.
[12] G.J. Wasserburg, S.B. Jacobsen, D.J. DePaolo, M.T. McCullough, J. Wen, Precise determination of Sm/Nd ratios, Sm and Nd isotopic abundances in standard solutions, Geochim. Cosmochim. Acta 45 (1981) 2311–2323.
[13] J.P. Bird, A.L. Clark, Microprobe study of olivine chromitites of the Good News Bay ultramafic complex, Alaska, and the occurrence of platinum, US Geol. Surv. J. Res. 4 (1976) 717–725.
[14] Y. Niida, Y. Terai, S. RahimKhan, A.B. Kausar, Origin of chromitites from the Jijal complex, Kohistan arc, north Pakistan, Geol. Bull. Peshawar, Pakistan 31 (1998) 140–141.
[15] H.J.B. Dick, T. Bullen, Chromian spinel as a petrogenetic indicator in abyssal and alpine-type peridotites and spatially associated lavas, Contrib. Mineral. Petrol. 86 (1984) 54–76.
[16] S. Arai, Chemistry of chromian spinel in volcanic rocks as a potential guide to magma chemistry, Mineral. Mag. 56 (1982) 173–184.
[17] R.G. Berman, Internally-consistent thermodynamic data for minerals in the system K_2O-Na_2O-CaO-MgO-FeO-Fe_2O_3-Al_2O_3-TiO_2-SiO_2-C-H_2-O_2, J. Metamorph. Geol. 8 (1988) 89–124.
[18] M. Dungan, A microprobe study of antigorite and some serpentinites pseudomorphs, Can. Mineral. 17 (1979) 771–784.
[19] A.E. Boudreau, E.A. Mathez, I.S. McCallum, Halogen geochemistry of the Stillwater and Bushveld Complexes; Evidence for transport of the platinum-group elements by Cl-rich fluids, J. Petrol. 27 (1986) 967–986.
[20] C.L. Chou, D.M. Shaw, J.H. Crocket, Siderophile trace elements in the Earth's oceanic crust and upper mantle, J. Geophys. Res. 88 (1983) A507–A518.
[21] K. Gueddari, M. Piboule, J. Amosse, Differentiation of platinum-group eements (PGE) and of gold during partial melting of peridotites in the lherzolitic massif of the Betico-Rifean range (Ronda and Beni Bousera), Chem. Geol. 134 (1996) 181–197.
[22] M. Roy-Barman, C.J. Allègre, $^{187}Os/^{186}Os$ ratios of mid-ocean ridge basalts and abyssal peridotites, Geochim. Cosmochim. Acta 58 (1994) 5043–5054.
[23] D.C. Peck, R.R. Keays, R.J. Ford, Direct crystallization of refractory platinum-group element alloys from boninitic magmas; Evidence from western Tasmania, Aust. J. Earth Sci. 39 (1992) 373–387.
[24] K. Hattori, S.R. Hart, PGE and Os isotopic signatures for ultramafic rocks from the base of the Talkeetna island arc, Alaska, EOS Trans. Am. Geophys. Union 78 (1997) F-339.
[25] K. Hattori, T. Shirahase, Platinum group elements and osmium isotope signatures of Kohistan Island Arc Sequence, Himalaya-Korakaram Area, EOS, Trans. Am. Geophys. Union, Fall Mtg. 78 (1997) F-829.
[26] D.J. De Paolo, Neodynium Isotope Geochemistry. An Introduction, Springer-Verlag, New York, 1988, 187 pp.
[27] T. Ishii, P.T. Robinson, H. Maekawa, R. Fiske, Petrolog-

ical studies of peridotites from diapiric serpentinites seamounts in the Izu-Ogasawara-Mariana Forearc, Leg 125, Proc. Ocean Drilling Prog. Sci. Results 125 (1992) 445–463.

[28] D.A. Ionov, V.S. Prikhod'ko, S.Y. O'Reilly, Peridotite xenoliths in alkali basalt from the Sikhote-Alin, southeastern Siberia, Russia trace-elements signatures of mantle beneath a convergent continental margin, Chem. Geol. 120 (1995) 275–294.

[29] A. Whittington, N.B.W. Harris, M.W. Ayres, G. Foster, Tracing the origins of the western Himalaya: an isotopic comparison of the Nanga Parbat massif and Zanskar Himalaya, in: M.A. Khan, P.J. Treloar, M.P. Searle, M.Q. Jan (Eds.), Tectonics of the Nanga Parbat Syntaxis and the Western Himalaya, Geol. Soc. Spec. Pub. 170 (2000) 201–218.

[30] S. Schwartz, P. Allemand, S. Guillot, Numerical model of the effect of serpentinites on the exhumation of eclogitic rocks: Insights from the Monviso ophiolitic massif (Western Alps), Tectonophysics 341 (2001) in press.

[31] T. Reinecke, Very-high pressure metamorphism and uplift of coesite-bearing metasediments from the Zermatt-Saas zone, Western Alps, Eur. J. Mineral. 3 (1991) 7–17.

[32] S.M. Peacock, Large-scale hydration of the lithosphere above subducting slabs, Chem. Geol. 108 (1993) 49–59.

[33] S.M. Peacock, R.D. Hyndman, Hydrous minerals in the mantle wedge and the maximum wedge and the maximum depth of subduction thrust earthquakes, Geophys. Res. Lett. 26 (1999) 2517–2520.

[34] Y. Furukawa, Depth of the decoupling plate interface and thermal structure under arcs, J. Geophys. Res. 98 (1993) 20,005–20,013.

[35] S. Kamiya, Y. Kobayashi, Seismological evidence for the existence of serpentinized wedge mantle, Geophys. Res. Lett. 27 (2000) 819–822.

[36] E. Bailey, J. Holloway, Experimental determination of elastic properties of talc to 800°C, 0.5 GPa; calculations of the effect on hydrated peridotite, and implications for cold subduction zones, Earth Planet. Sci. Lett. 183 (2000) 487–498.

[37] K. Wang, T. Mulder, C. Rogers, R.D. Hyndman, Case for very low coupling stress on the Cascadia subduction fault, J. Geophys. Res 100 (1995) 12,907–12,918.

[38] N. Carter, M. Tsenn, Flow properties of continental lithosphere, Tectonophysics 136 (1987) 27–63.

[39] C.T. Klootwijk, J.S. Gee, J.W. Peirce, G.M. Smith, P.L. McFadden, An early India-Asia contact paleomagnetic constraints from Ninety East Ridge, ODP Leg 121, Geology 20 (1992) 395–398.

[40] S. Duchêne, J.M. Lardeaux, F. Albarère, Exhumation of eclogites: Insights from depth-time path analysis, Tectonophysics 280 (1997) 125–140.

[41] L. Savostin, J. Sibuet, L. Zonenshain, X. Le Pichon, M.J. Roulet, Kinematic evolution of the Tethys belt from the Atlantic ocean to the Pamirs since the Triassic, Tectonophysics 123 (1985) 1–35.

[42] A.I. Shemenda, Horizontal lithosphere compression and subduction: constraints provided by physical modeling, J. Geophys. Res. 97 (1992) 11097–11116.

[43] M. Toriumi, Flow under the island arc of Japan and lateral variation of magma chemistry of Island arc volcanoes, J. Phys. Earth 26 (1978) 423–435.

[44] J. Escartin, G. Hirth, B. Evans, Nondilatant brittle deformation of serpentinites: implications for Mohr-Coulomb theory and the strength of faults, J. Geophys. Res. 102 (1997) 2897–2913.

[45] E.H.H. Strating, R.L.M. Vissers, Dehydration-induced fracturing of eclogite-facies peridotites implications for the mechanical behavior of subducting oceanic lithosphere, Tectonophysics 200 (1991) 187–198.

[46] B.R. Hacker, Eclogite formation and the rheology, buoyancy, seismicity, and H_2O content of oceanic crust, in: G.E. Bebout, D.W. Scholl, S.H. Kirby, J.P. Platt (Eds.), Subduction Top to Bottom, Geophys. Monogr. Series 96 (1996) 337–346.

[47] W. McDonough, S.S. Sun, The composition of the earth, Chem. Geol. 120 (1995) 223–253.